PRELIMINARY STEPS IN THE DEVELOPMENT OF DOPPLER GLOBAL VELOCIMETRY AT VKI

Carlo Bagnera   Daisaku Sakaguchi   Doug Fletcher

von Karman Institute for Fluid Dynamics

Turbomachinery and Propulsion Department

Chaussée de Waterloo 72, 1640 Rhode St Genèse, Belgium

bagnera@vki.ac.be

ABSTRACT

The principle at the base of the Doppler Global Velocimetry is explained. Details of the physics of an Argon ion laser are discussed with a view to the implementation of this new technique. To insure monomode running of the laser and frequency tuning capabilities, an etalon is installed inside the laser cavity. The development of two iodine cells with different characteristic is presented, along with calibrations for different temperatures. The role of the long and short time stability of the laser frequency is considered. Measurements of an axisymmetric jet are performed with an accuracy contained in the range of ±3m/s.

INTRODUCTION

DGV (Doppler Global Velocimetry) is a system to measure velocity of particles crossing a laser sheet, by analyzing the scattered Doppler shifted frequency of a light sheet. The light frequency shift is very weak because of the very low speed of the particles compared to the speed of light. In order to overcome this problem, an absorption line of the molecular iodine is used: the absorption of iodine depends strongly on the light frequency going through the iodine vapor. By this mean, it is possible to measure the scattered light intensity going through the iodine and normalize it to the scattered light: this ratio gives us the percentage of light absorbed by the iodine and therefore the Doppler shifted frequency. The frequency shift can be traced back to particle velocity.

The continuously growing CFD methods drive the interest of the studies of 3 dimensional flows, which arises then the interest of the researchers in the development of 3 dimensional measurement techniques. The basic principle of the DGV system is easily extensible to measure the 3 components of velocity since out-of-plane motion of particles poses no problems, in contrast to the general optical planar measurement techniques. Table 1 shows the comparison of advantages and disadvantages between PIV and DGV.

The basic principle of DGV has been patented by Komine [1] in 1990. Since then, Meyers [2] at the NASA-Langley research center took over the idea and devoted many efforts in the development of this promising 3-dimensional measurement technique.

NOMENCLATURE

c : velocity of light

$\vec{l}$: unit vector of laser beam direction

L : length of laser resonator

ΔL : mirror displacement

υ_0 : laser frequency

υ : scattered light frequency

$\Delta \upsilon$: Doppler shift

$\vec{o}$: unit vector of observation direction

t : thickness of etalon

θ : tilting angle

$\vec{V}$: velocity vector of the particle

Table 1 Comparison of DGV and PIV

	DGV	*PIV*
SEEDING	+ independent of seeding concentration	- requires good seeding concentration
CAMERA	+ no high-resolution required + endoscopes, optical fiber bundles	- "interrog. window" limited resolution - better not
PROCESSING	+ almost on-line	- lengthy processing
VELOCITY COMPONENT	+ any flow direction + 1C, easy 3C	- in-plane flow - 2C, difficult 3C
READY TO USE	- under heavy development	+ consolidated
INSTAN-TANEOUS	- Nd:YAG (higher bandwidth)	+ intrinsically
STATISTICS	- average measurements	+ average & statistics

DGV SYSTEM: BASIC PRINCIPLE

The principle of DGV is based on the detection of light scattered by the particles that seed the flow. Due to the velocity of the particles, the scattered

light frequency is Doppler shifted according to the following equation:

$$\Delta \upsilon = \upsilon - \upsilon_0 \qquad (1)$$

The following formula shows the relationship among the frequency shift $\Delta \upsilon$, the particle velocity $\vec{v}$, the direction of the laser $\vec{l}$ and the direction of observation $\vec{o}$:

$$\Delta \upsilon = \upsilon_0 \frac{(\vec{o} - \vec{l})}{c} \cdot \vec{v} \qquad (2)$$

moreover, figure 1 shows the geometrical relationship among these parameters.
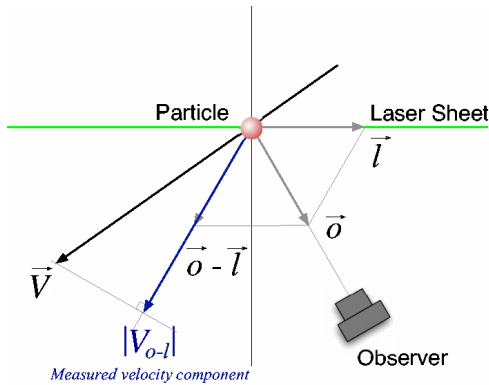
Figure 1 Determination of measured velocity component direction

Velocity of light, c, is much bigger than the velocity of the particles, $\vec{v}$, therefore the Doppler shift, $\Delta \upsilon$, is extremely small: in order to measure this small frequency changes, an absorption line of molecular iodine is used. Vapor iodine is contained in a glass reservoir, called iodine cell. When scattering light goes through this iodine cell, strong changes of light intensity can be noticed according to the incoming light frequency. Figure 2 shows the absorption line of iodine calculated using the simulation program. The well known wavelengths of argon ion lasers at 514.5 nm or Nd:YAG lasers at 532 nm are available. Two detectors are required to measure the scattered light intensity before and after the iodine cell. When using a CCD as a detector, the intensity ratio can be analyzed for each pixel and the velocity field can be obtained in the light sheet plane. In order to achieve the 3 dimensional measurements, a light sheet direction change or an observation direction change is required. The use of a continuous wave laser, like the Ar^{+} laser, leads to averaged measurements, while the use of a pulsed laser, like a Nd:YAG laser, allows unsteady measurements. Works of Smith [3], McKenzie [4], Fischer [5], and Elliott [6] are examples of Nd:YAG laser applications, while works of Meyers [2,7], Ainsworth [8] and Roehle [9] are examples of Ar^{+} laser applications
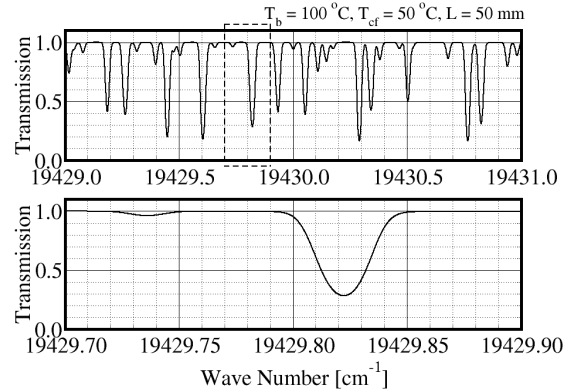

Figure 2 Simulation of absorption line for molecular iodine

SYSTEM SET-UP

LASER SOURCE

Figure 3 shows the system set-up for the calibration of the iodine cell. The laser source consists of a Spectra Physics 5 W Ar^{+} laser model 2020. A triangular prism is installed in the laser cavity in order to allow only the green line (514.5 nm) to lase. The maximum output power of this single line configuration reaches 2.5 W.
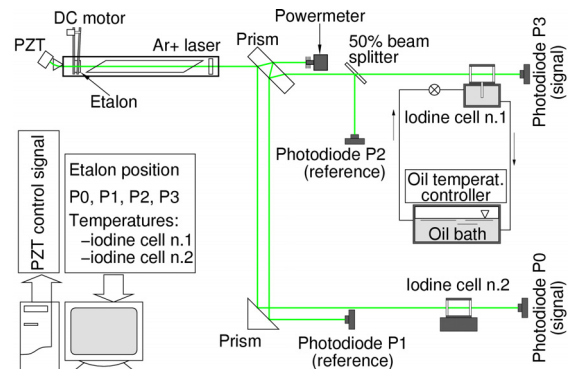

Figure 3 DGV System set-up for calibration of the iodine cell

Figure 4 shows the gain profile of a typical Ar^{+} laser. The green line contains around 23 modes. The separation between the lines is called *Free Spectral Range (FSR)* and is defined by the formula:

$$FSR = \frac{c}{2L} \qquad (3)$$

The laser used for this project has a resonator around 1 m long, which gives a *FSR* of 150 MHz.

A Fabry-Perot etalon is used for monomode running. Figure 5 shows a sketch of the etalon installed in the laser cavity: the etalon works as a second resonator inside the laser cavity. The etalon consists of two wedged plates, each having one high reflection and one antireflection coating. When the etalon is placed inside the laser cavity, mode competition effects enhance the etalon ability to select a particular frequency. Tilting the etalon

2

affects the light path length inside the etalon resonator and this allows a frequency tuning: bigger tilting angles correspond to shorter wavelengths of the light and therefore to higher frequencies. Two different kinds of etalon exist: an air spaced model and a temperature stabilized model. The working principle of the two models is different: in the case of an air spaced etalon, a spring acting on the resonator changes the index of refraction of the resonator; while in the case of a temperature stabilized etalon, the light path length inside the resonator is controlled by the dilatations due to heating. In this project, an air spaced etalon (Spectra Physics Model 589 Air Spaced Etalon) was used, as in previous work by Meyers [7]. In order to be able to tilt the etalon by very small angles, the Spectra Physics system has been modified, extending the arm-support and introducing a DC motor with a rotary encoder. In this way the tilting angle can be monitored by a computer. The minimum resolution achievable is 0.14×10^{-3} deg.
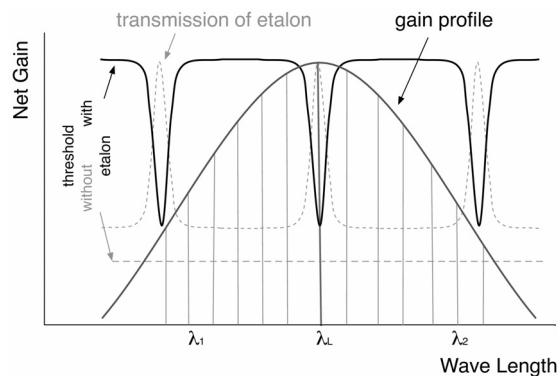

Figure 4 Gain profile, resonator modes and transmission peaks of the intracavity etalon (dash curve). Also shown the threshold curves with and without etalon

The following equation shows the *FSR* of the etalon:

$$FSR = \frac{c}{2t\cos\theta} \qquad (4)$$

with a thickness of the etalon of 15 mm and a tilting angle equals to 0 deg this formula gives a *FSR* of 10 GHz.

IODINE CELLS

Figure 6 shows the iodine cells. Two cells have been successively developed: both of them are made by a cylindrical glass reservoir with an internal diameter of 35.4 mm and a length of 50 mm. They are rolled up with a current controlled heating wire to stabilize the temperature of the cell body (usually kept at 100ºC). A cylindrical teflon cover insures adiabatic conditions of the cell body. The first cell has a second smaller reservoir attached vertically at the bottom of the main cylindrical body: this is usually kept at a

temperature colder than the main body, and therefore called 'cold finger'. The whole is sealed under vacuum condition with a bead of solid iodine inside, in a similar way to the procedure described by Ford and Tatam [10]. The cold finger is immersed in a plexiglass oil bath with circulating oil for a fine temperature control. This temperature determines the sublimation level of the solid iodine. A precise temperature control (±0.1 deg) is required, since the sublimation level strongly depends on the temperature. To monitor the cell temperature, three thermocouples are installed: two on the main body and one on the cold finger. The second cell was initially manufactured as the first, but then the cold finger has been cut away, while the whole cell was kept at a design temperature of 60ºC. Care was taken in order to keep what was left of the solid iodine in the 'cold finger'. The result is a cell with a limited amount of iodine contents. Four thermocouples are installed around the cell body, for accurate temperature monitoring.

An extensive and exhaustive discussion on iodine cells for Doppler Global Velocimetry has been published by Chan et al. [11].
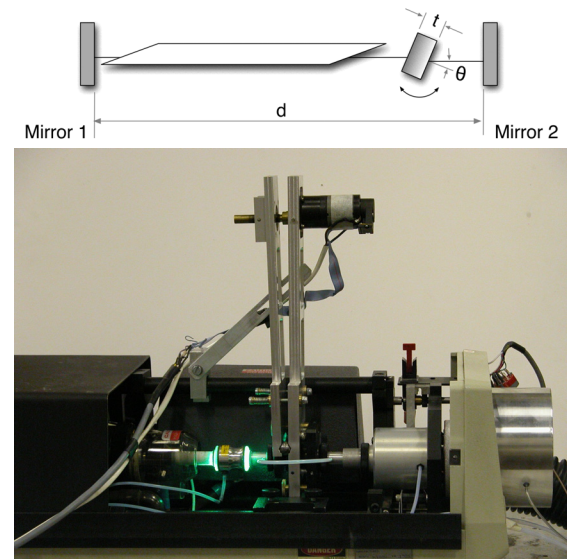

Figure 5 Etalon system inside the laser resonator. Single-mode operation by inserting a tilted etalon (top). Photo of the etalon-tilting device designed by von Karman Institute (bottom)

LIGHT DETECTORS

The first goal of this project is the successful achievement and the accuracy check of one-component velocity measurements. The first approach took into consideration only point-wise measurements, and for this reason a photodiode is enough. The photodiodes used in this research are Hamamatsu S2386 with an effective active area size of 3.6x3.6 mm. The light scattered by the particles is collected by a receiving optic and then split into two parts by a 50% beam splitter: one

3

beam will be the reference to be read by one photodiode, I_0, and the second one, going through the iodine cell, will be the signal, I. The amplified signals of the photodiodes are acquired by a computer and the ratio I/I_0 is computed, so that the conversion from intensity ratio to velocity can be done using the calibration of the iodine transmission curve. The scattering particles are generated with a smoke generator developed at von Karman Institute: if propylene glycol is used as a liquid, particles smaller than 1 μm can be obtained.

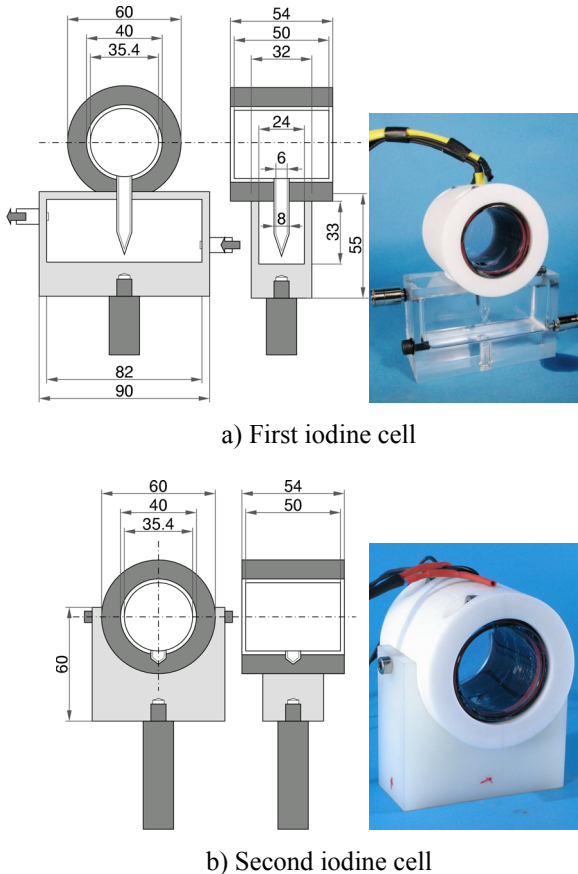a) First iodine cell

b) Second iodine cell

Figure 6 Iodine cells manufactured by von Karman Institute.

ACQUISITION SYSTEM

The analog signals are recorded on a computer by means of a 16 bit AD acquisition card Keithley KPCI-3108. A maximum of 8 channels can be acquired simultaneously. The sampled channels where decided according to the test, in order to measure the photodiode signals and to monitor the temperatures of the cells, the ambient temperature, and a rotary encoder (to monitor the etalon position, at calibration time).

CALIBRATION OF THE IODINE CELL

MODE SWEEPING

Figure 7 shows the output of the photodiodes and the intensity ratio distribution versus etalon angle variation. Tilting the etalon away from the center of the optical axis moves the laser light towards higher frequencies, such that the laser modes are swept. The etalon transmission has a frequency distribution around its central value defined by the `Full Width at Half Maximum' of the line, $FWHM$. The laser mode which sees the highest etalon transmission within the $FWHM$ will oscillate. The signal from the reference photodiode I/I_0 shows the sweeping of the Ar^+ modes. The FSR of the etalon is 10 GHz and the gain profile of the green line of an Ar^+ laser is about 3.5 GHz. Since the etalon FSR is wider than the green line gain profile of the laser, some etalon positions correspond to no light. The rest part of the curve are showing the gain profile of the laser. When the trend of the gain profile is decreasing, the signal I shows very strong variations because of Rayleigh scattering inside the iodine cell.
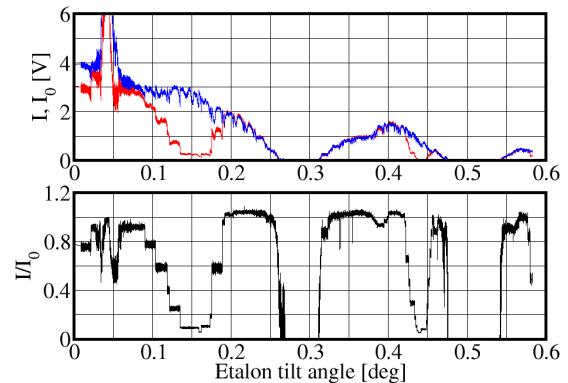

Figure 7 Photodiode output signals and intensity ratio distribution versus etalon angle variation

TRANSMISSION CURVE AND TEMPERATURE DEPENDANCY

Figure 8 shows a close-up of the first absorption line of figure 7, translated to a frequency axis arbitrarily set to zero in the center of the absorption curve. The two curves represent respectively the intensity ratios as seen from the first and the second iodine cell. The stepwise intensity ratio changes are clearly recognizable: they are the mode hops of the laser frequency, and they correspond for the two cells to the same etalon tilt angle. The difference in the y direction is to be traced back at the different iodine vapor concentration in the cell. Both the negative and positive slopes present 7 to 10 steps in this case. The central point is considered representative of each step: the transmission curve can be reconstructed by interpolating the successive points.

Each wing of the absorption curve presents a linear character in its middle. Figure 9 shows the same plot of mode sweeping for 4 different cases recorded with the first cell. Small differences between cases can be noticed because of slightly different temperature conditions of the iodine cell, nevertheless a very high repeatability could be achieved.
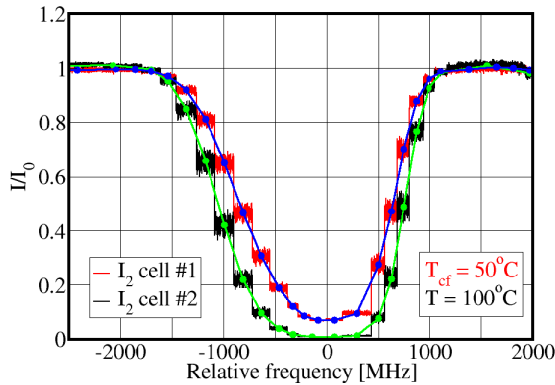

Figure 8 Measured intensity ratio showing mode hops at T_{cf} =50ºC

Figure 10 shows the iodine transmission curve of the first iodine cell for different temperature values of the cold finger. The graph shows a strong dependence of the transmission curve on the cold finger temperature, therefore the cold finger temperature needs to be precisely controlled. A value of 50°C was selected as the most suited for measurements and a variation as small as ±0.2°C was achieved over a monitoring time of one hour.
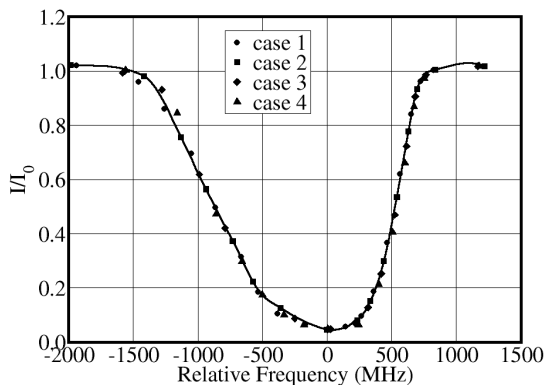

Figure 9 Measured intensity ratios for different cases and interpolating line at T_{cf} =50ºC

The accurate temperature control of the cell is overcome by using the second iodine cell: figure 11 shows the transmission curve of the second iodine cell for different temperatures. A good repeatability of the iodine transmission curve for temperatures above 90ºC could be achieved. The conditions in the cell do not vary when all the iodine is in the vapor phase. For a cell body temperature of 80ºC not all the iodine is vapor and the absorption line changes shape as can be read in figure 11. For a

cell body temperature of 70ºC a clear formation of solid iodine appears in the center of the optical glass.
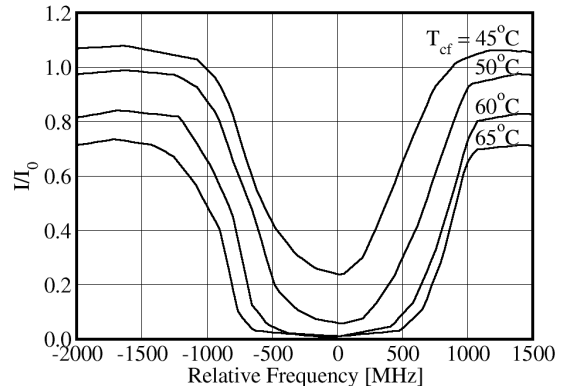

Figure 10 Measured intensity ratios through iodine cell n.1 for different cold finger temperature values

In order to perform measurements, the etalon angle has to be set in such a way as to tune the laser frequency in the center of one of the two linear wings of the absorption line. The sign of the two wing slopes are opposite: the left part has a negative slope, while the right part has a positive slope. The absolute value of the two slopes is also different: the right part is steeper than the left part. At a cold finger temperature equals to 50°C, the linear sections of the left and right wings extend over a range of 500 MHz and 250 MHz respectively. The selection of the wing should be made according to the dynamic range of the flow to be measured. In other words, a certain velocity produces a bigger intensity ratio variation if measured on the right wing than on the left wing, resulting in a higher accuracy measurement.
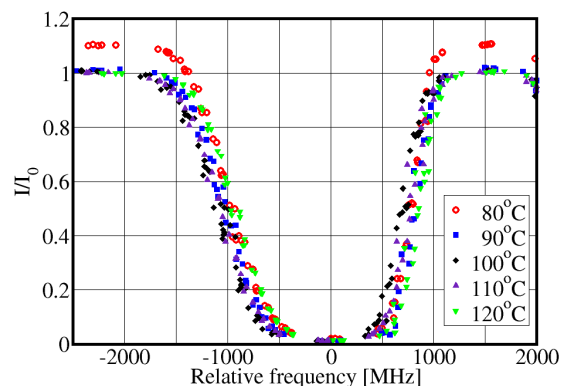

Figure 11 Measured intensity ratios through iodine cell n.2 for different cell temperature values

STABILITY OF MONOMODE

Figure 12 shows a one-hour time history graph of the intensity ratio at the middle point of the iodine transmission curve monitored with the first cell. The sampling rate was set to 5 Hz. The upper graph shows the intensity ratio I / I_0 and the lower

5

graph shows the temperature of the main body of the iodine cell T_b, the temperature of the cold finger T_{cf} and the ambient temperature T_{amb}. The trend of the temperature is constant and the range of fluctuation is ±0.2°C, nevertheless the intensity ratio presents a saw tooth shape, due to mode hops in the laser cavity. The time lag between mode hops is not always constant. The strength of the jumps can be estimated around 150 MHz taking into consideration an intensity ratio change of the order of 0.3 and the right wing of the first iodine transmission curve at T_{cf} = 50°C. This frequency change is a reasonable value because it corresponds to the *FSR* of the laser cavity length in use. This is sure not a negligible change in the laser frequency at measurement time. The reason for the sudden changes has to be looked for elsewhere: possible alternatives are variations of the cooling water temperature, changes of the cooling water flow rate, mechanical vibrations of the laser frame or variations of the current of the power supply. An accurate control of all these parameters would increase the complication level of the system.
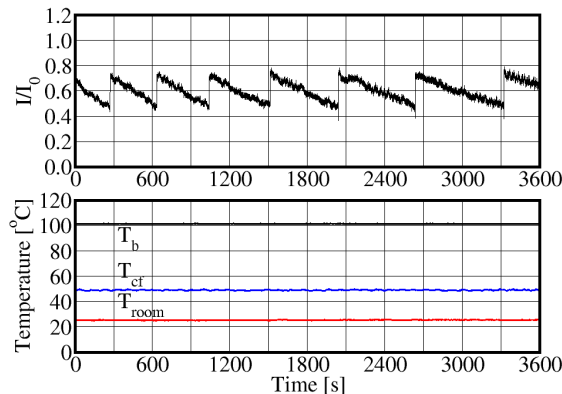
Figure 12 Time history of intensity ratio at the middle point of iodine transmission curve

In order to avoid this mode hopping, two methods are possible: short time measurements or active control of the laser cavity length. In the frame of this work, the former solution has been adopted. Figure 13 shows a 20 s time history graph of intensity ratio at the middle point of iodine transmission curve and a power spectrum distribution of the fluctuations. The rate of intensity ratio decrease is 0.1% over a 20 s period, which corresponds to 6.7 MHz taking into consideration an iodine transmission curve at T_{cf} = 50°C. The lower graph shows the power spectrum distribution. The highest power content is in a peak at 75 Hz, which does not correspond to the network frequency (50 Hz). The mode hop and the frequency drift are not acceptable for long time measurements and a way to overcome this unwanted effect has to be found.
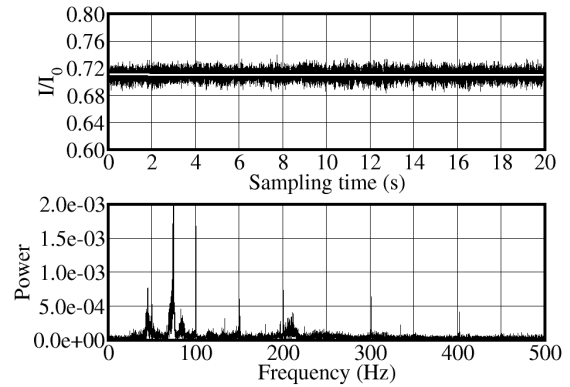
Figure 13 Time history of intensity ratio at the middle point of iodine transmission curve at T_{cf} =50ºC

A future solution would be the use of a piezo translator, which displaces one of the cavity mirrors for an active control of the cavity length, as reported by the work of Roehle [9]. Such a system has been installed on the rear mirror of the laser in use. It consists of a piezo translator Physik Instrumente Model S-310.10 that has been mounted on a modified mirror support designed at von Karman Institute. The piezo should be driven with a phase opposite to the laser output. The changes of laser frequency can be related to the changes in the cavity length with the following formula:

$$\Delta \upsilon = \upsilon_0 \frac{\Delta L}{L} \tag{5}$$

The piezo translator has a minimum resolution of 0.1 nm and a maximum displacement of 6.0 μm, which correspond to a frequency variation of 0.6 MHz and of 3.5 GHz respectively.

MEASUREMENTS OF A CIRCULAR JET

Figure 14 shows the experimental set-up for the measurement of the circular jet. The circular jet has a diameter d of 11.3 mm and has been located under an angle of 45° with respect to the laser light direction. The measurement point is in the center of the jet, 1.24 d downstream the circular pipe exit. The nozzle has a pressure tap in the settling chamber that has been calibrated with the velocity of the jet. Simultaneous recordings of the settling chamber pressure and velocity measurements are performed. The diameter of the laser beam is 1.7 mm and the measurement volume correspond to 4mm obtained taking into account the effective photodiode area size and the position of the receiver lens. Previous characterization of the jet indicates that the measurement volume is inside the potential core of the jet. The measurements were performed over a time period of 20 s; the velocity of the jet was varied continuously from 10 to 50 m/s and back within the measurement time. The sampling frequency is 1 kHz; the continuously sampled data has been averaged every second into

6

one single point. The laser frequency was set on the middle point of the left wing of the iodine transmission curve. Figure 15 shows the experimental results for four different cases compared to the velocity calculated from the settling chamber pressure. The points are spread over a range of ±3 m/s. These results are in agreement with the early work of Roehle [12].
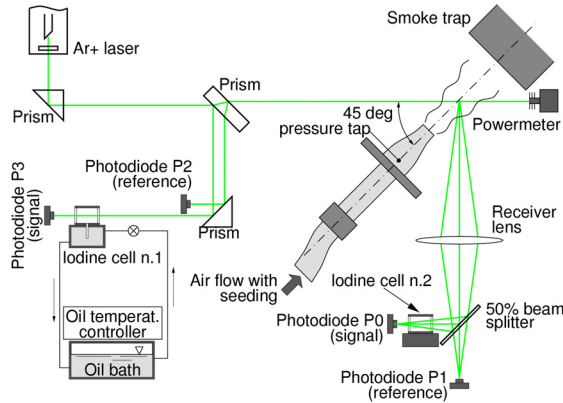

Figure 14 Experimental set-up for the measurements of the circular jet
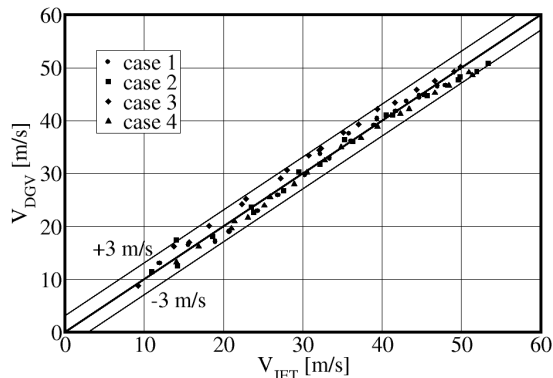

Figure 15 DGV measurements versus total pressure probe measurement, and accuracy range

CONCLUSION

The first steps in the development of a DGV system have been set. The design of two iodine cells proved to be working. The etalon tilting device allowed short time calibrations of the iodine cell with high repeatability. One-component velocity measurements have been performed in the core of a circular jet with an accuracy contained in a range of ±3 m/s. The future work of the frequency stabilization with a piezo translator has been discussed. The future work involves also the extension of the system to planar measurements by means of a CCD camera and the extension to three component measurements. The DGV measurement technique requires the monitoring of many parameters: the reduction of the number of

parameters is the key point which may open the way of the wide spreading of this technique in fluid dynamics laboratories.

REFERENCES
[1] Komine H. System for measuring velocity field of fluid flow utilizing a laser-doppler spectral image converter U.S. Patent no. 44919536, April 24 1990
[2] Meyers J.F. and Komine H. Doppler global Velocimetry: a new way to look at velocity. In Fourth International Conference on Laser Anemometry, Cleveland, USA, January 7-10 1991
[3] Smith M.W., Northam G.B and Drummond J.P. Application of Absorption Filter Planar Doppler Velocimetry to sonic and supersonic jets. AIAA Journal, Vol. 34, No. 3, March 1996
[4] McKenzie R.L. Planar Doppler Velocimetry performance in low-speed flows. AIAA paper 97-0498 in 35th Aerospace Sciences Meeting & Exhibit, Reno, NV, USA, January 1997
[5] Fischer M., Heinze J., Matthias K., and Roehle I. Doppler Global Velocimetry in flames using a newly developed, frequency stabilized, tunable, long pulse Nd:YAG laser. In 10th Int. Symposium on Applications of Laser Techniques to Fluid Mechanics, Lisbon, Portugal, July 2000
[6] Elliott G.S. Samimy M. Arnette S.A. Molecular filter based Velocimetry technique for high speed flows. Experiments in Fluids, 18:107-118, 1994
[7] Meyers J.F. Doppler Global Velocimetry. The next Generation? In AIAA 17th Aerospace Ground Testing Conference, Nashville, TN, USA, July 6-8, 1992
[8] Ainsworth R.W., Thorpe S.J. The development of a Doppler global velocimeter for transonic turbine applications. In Int. Gas Turbine and Aeroengine Congress and Exposition, 94-GT-146, The Hague, Netherlands, June 1994
[9] Roehle I. VKI-Lecture on: Doppler Global Velocimetry. In Advanced Measurement Techniques VKI LS 1998-06, April 6-9, 1998
[10] Ford H.D. Tatam R.P. Development of Doppler Globabl Velocimetry for Turbomachinery applications. In 8th international symposium on applications of laser techniques to fluid mechanics, Lisbon, Portugal, July 8-11, 1996
[11] Chan V.S.S. et al. Iodine absorption filters for Doppler global velocimetry. Meas. Sci. Technol. Vol. 6 (1995) pp. 784-794
[12] Roehle I, and Schodl R. Evaluation of the Accuracy of the Doppler Global Technique. In Optical Methods and Data Processing in Heat and Fluid Flow, London, UK, April 14-15 1994

7